
ISSN: 2321-2152
IJMECE
International Journal of modern electronics and communication engineering
E-Mail
editor.ijmece@gmail.com
editor@ijmece.com
www.ijmece.com

ISSN2321-2152
www.ijmece .com
Vol 12, Issue 1, 2024

Investigating the Use of Frequency-Domain Correlation Technique for Dynamic Response Assessment of RC Bridge Piers and Impact Damage Detection

Mr. K. Sedhuramalingam, Mr. S. Samraj, Mrs. K. Devadharshini, Mrs. D. Chitra

Assistant Professor [1,2,3,4]

sedhuramalingam.k@actechnology.in, ssamraj@actechnology.in, devadharshini.k@actechnology.in, chitra@actechnology.in

Department of MCT, Arjun College of Technology, Thamaraikulam, Coimbatore-Pollachi Highway, Coimbatore, Tamilnadu-642 120

ABSTRACT:

We investigated the potential applications of damage correlation indices, which are correlation techniques based on the frequency domain, to enhance damage detection in reinforced concrete columns. Researchers used a new ultra-high drop hammer experiment method to hit four miniature reinforced concrete pier components, simulating the impact of medium-sized cars on bridge piers. The members' frequency response functions were assessed before and after the damage using an acceleration acquisition device. Damage correlation indexes (DCI) taking multi-order modal frequencies into account provided reasonable estimates of the pier damage levels, according to the studies. In addition, a modal analysis method and an impact finite element model were built and matched with the trials using the commercial program LS-DYNA. The impact processes between medium-sized automobiles and reinforced concrete piers were simulated by matching the finite element parameters with the experimental data. In order to guarantee that the structural design requirements are satisfied, a computation for the peak impact force (PIF) was provided for vehicle accident scenarios using damage indices.

Modal frequencies, reinforced concrete piers, numerical models, damage detection, and lateral impacts are some of the most important terms in this context.

I.INTRODUCTION

The number of people living in cities has increased dramatically due to the accelerated pace of urbanisation.

region's automobiles and transportation infrastructure. As a result, the primary danger to the security of urban overpasses now comes from car accidents with bridge piers. Numerous statistical studies on serious accidents caused by bridge collapses since the turn of the century have shown that incidents involving ships or vehicles striking bridges constitute around 20% of these events.1 Particularly relevant in these instances are the uses of structural health detecting technologies. The massive financial outlay required for damage assessments and restoration procedures could impede the execution of required measures. The advancements in sensor and computer technology have really led to better options for damage assessments in terms of solutions. New technologies, such as vibration-based monitoring systems, let engineers gather data in real-time, enabling real-time evaluation of structures by comparing original and damaged condition characteristics.2 In terms of data use, natural frequencies3, modal shapes4, mass values5, stiffness values6, damping matrices7, and frequency response functions (FRFs) rank high.8

There have been many countries that have proposed design codes to address the impact issues. The suggested AASHTO LRFD,9 which uses the comparable static force, is the most typical code.

with a distance of 1500 mm from the road edge and a design value of 2670 KN for the bridge piers. To test its reasonableness, we utilised the preliminary rough finite element model developed by Chen et al.10. The findings revealed that, in some instances, the values employed in the code were too cautious. So, the numbers given earlier were checked using the finite element model suggested by Abdelkarim and ElGawady11. We also compared these results with those from the equivalent static force calculation technique (equation) and the 25 ms average peak force approach.

Euro-code has suggested (1).12 According to the findings, the corresponding static force for structural designs should be the average of the 25 ms peak force that was suggested by Buth et al.13.

$$\mathrm{ESF} = \frac{m v_{\mathrm{r}}^{2}}{2(\delta_{\mathrm{C}} + \delta_{\mathrm{D}})} \qquad (1)$$

The variables m, Vr, dc, and dD stand for the vehicle's mass, velocity, distance from its head to its centre of mass, and transverse deformation (dD) at the moment of collision. A full-scale rigid pier model was subjected to transverse impact studies by Buth et al.14 using a 36t tractor-semitrailer. The model graphically displayed the mechanical behaviours of the bridge pier, such as the collision with the cargo pier and the crushing of the vehicle's head. In order to conduct transverse impact trials, Chen et al.15 built a five-column anti-collision guardrail and tested it using a medium-sized Dongfeng-EQ140 truck. Various metrics, including impact force and deflection, were documented throughout the testing procedures. A simpler finite element guardrail model was then proposed using the experimental data that had been gathered. In their study, Cai et al.16 used a transverse impact experimental equipment to conduct impact tests on 15 square scale columns. The aforementioned research primarily focused on the impacts of slenderness ratios on impact energy, peak impact force, and member deformations. The similar investigation by Zhou et al.17 investigated the changing reactions of used an experimental setup with an extremely high drop hammer to test concrete pier elements subjected to cumulative impact settings. The findings indicated that the buildings' internal energy dissipation capabilities had been steadily declining as damage degrees increased, and a modal frequency change-based damage judgement approach was suggested. Without a shadow of a doubt, the advancement of numerical models in this area has been substantially aided by previously executed impact tests. While conducting weight reduction experiments on reinforced concrete beams, Adhikary et al.18 developed a comprehensive finite element model to examine several factors such as impact mass ratios, longitudinal reinforcement ratios, concrete compressive strength, and more. Furthermore, Pham and Hao19 verified the assumption of linear inertial force distributions along beams, developed a numerical model of reinforced concrete beams, and simplified the mechanical model to better capture the dynamic behaviours of these structures during impact processes. They also suggested a way to derive shear and bending moment diagrams. The impact impacts of heavy vehicles and reinforced concrete columns may be replicated with the use of an impact frame that was created by Chen et al.20. The equivalency values between the frames and real trucks were then determined by comparing the deformations and internal energy relations of the two. Lastly, a suitable finite element simulation was set up to confirm their general similarity. The idea of performance-based design for impact concerns was put out by Sharma and al.21, who created finite element pier models for several vehicle impact scenarios. Furthermore, the damages were effectively identified under various conditions, and a suite of software frameworks was created to assess the capabilities and requirements of dynamic shear force in RC columns. But there isn't a suitable and trustworthy quantitative index, and the performance design criteria used to classify bridge pier safety grades are too imprecise. According to the research, a high-

damage assessment indices and impact forces were suggested to be used in a technique for calculating applicability. Trucks were used to conduct simplified impact testing on reduced-scale circular section piers in this study's trials. The RC columns' dynamic reactions to impact were recorded, as were the modal frequency shifts after member damage. Next, we utilised LS-DYNA software22 to confirm the experimental findings, and then we built a comprehensive finite element model based on those data. Additionally, a full-scale pier model was created using finite element analysis to simulate impact scenarios. Numerical simulations conducted for this research showed correlations between the peak effect

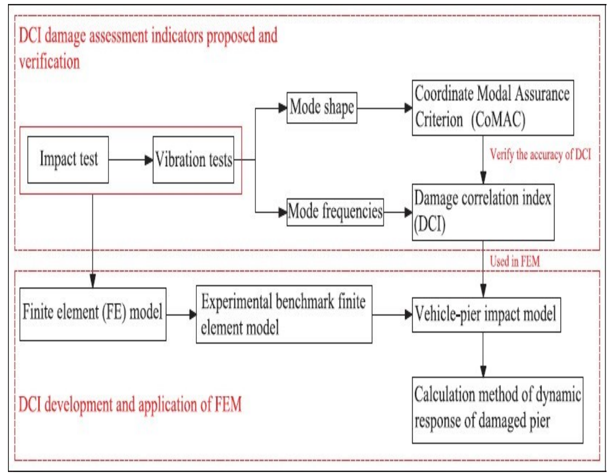

Figure 1. Technical route diagram of the experiments.

energy field (PIF) and the severity of the harm. A formula for the equivalent static force calculation of car hits in a short time was then developed, taking the bridge pier's age into account; this might serve as a useful reference for future structural designs. This article's research techniques are shown in Figure 1.

Damage assessment methods based on frequency domains

2. The change in dynamic response produced by the presence of damage is the foundation of the vibration-based impact damage assessment approach. Because of this occurrence, we can determine if harm has occurred as a result of the change in dynamic responsiveness. Under this part, two

many damage indication kinds are shown. Two such schemes are the Coordinate Modal Assurance Criterion (CoMAC) and the Modal Assurance Criterion (MAC)23.24 This indication shows how the mode shape deviates before and after the reinforced concrete structure is damaged. One key distinction is that COMAC takes into account deviations of multi-order mode shapes, while MAC just takes into account deviations of first-order mode shapes. The second one is known as the damage correlation coefficient (DCI), and it may show how the multi-mode frequencies changed before and after structural damage.

The target to be confirmed in this study is the damage index DCI suggested for impact damage, with CoMAC being

$$\mathrm{DCI} = 1 - |\mathrm{PCC}_{A,B}| \in R \qquad (7)$$

regarded as a conventional damage assessment index.

3. **MAC and CoMAC**
4. Equation (2) shows that the MAC, a dimensionally-invariant scalar constant, measures the degree of correlation between two modal vectors: one modal vector and another reference modal vector. For State A, the i-order modal vector is denoted by CAi in the equation. Its correlation is modal related, and it is an extension of the MAC known as the co-ordinate modal assurance criteria (COMAC)24. Equation (3) shows that at point i in State A, CAij is the j-order mode shape:

Damage correlation index (DCI)

In this research, the degree of damage was assessed by comparing the original modal frequency with the damage modal frequency and looking for parallels or differences. A comparison of the two samples was made using the numerical value. As for the specimen, Correlation by Pearson

The issue might be addressed using the PCC25 coefficient as a variance. In equation (4), we can see that A and B stand for the healthy and damaged states, respectively. In the healthy state, Ai is the i-th order modal frequency. In a healthy condition, A is the mean value of the frequency sample, and SA is the standard deviation within this sample:

For real numbers with PCC value of [21,1], 1 represents the linear correlation; 0 represents the complete correlation; and 21 represents the reverse or indirect correlation between the data sets compared. However, such cases do not appear in this study since they represent the reverse correlation of the frequency. Therefore, assuming that PCC is bounded in the range of [0, 1], the damage correlation coefficient DCI could be calculated. It was not difficult to determine that the value of DCI was 0 when the column was undamaged and 1 when the correlation was completely lost:

Experimental processes and analysis results Two stages were used to achieve this goal: first, a lateral member percussive impact system; second, a member after damage vibration test, which assessed modal characteristics; and lastly, the influence of the effective loss characteristic index was studied. This project involves the design of four components for bridge piers with a circular cross-section and a scale of 1:3. To scale the test model according to Buckingham's p theory, we refer to Section "Vehicle-bridge impact model," which provides the precise dimensions of the bridge pier model. Within the

During pouring, check that the materials used for the smaller parts match those for the larger bridge piers. The material properties' scaling impact is currently 1:1:

5. Procedures based on observation

The broken parts are prepared. Figure 2 displays the detailed specimens. The components of each specimen were an RC base measuring 900 3 300 3 400 mm3 and a 2200 mm tall circular RC column with a 170 mm section radius.

Oh, my. Concrete with a cube compressive strength of 42 MPa was used to cast all of the specimens.

In order to conduct the impact tests, the researchers used a system that consisted of a vertical drop-hammer driving system and a horizontal impact system (Figure 3). The horizontal impact test vehicle's kinetic energy was supplied by the vertical drop-hammer drive system, as shown in Figure 3(a). In equation (8), we can see the link between the two masses, m1 and m2, which stand for the steel impactor and drop weight masses, respectively. Here, g is the

ISSN2321-2152
www.ijmece .com
Vol 12, Issue 1, 2024

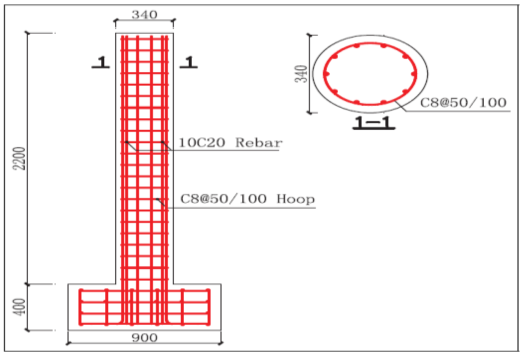

Figure 2. Specimen dimensions and detailed.

the track's dynamic friction coefficient, h stands for the drop weight's release height, and g is the acceleration of gravity. You may find the fundamental features of the experimental parts and the affecting strategy in Table 1. In terms of the column's dynamic reaction, the cumulative effect reflects the degree of damage:

Vibration tests. Damaged components were subjected to modal testing after impact in this investigation. Remove axial load to guarantee The higher part of the column is kept free from vibration, and the axial force is not used in the test. Figure 4(a) and (b) illustrate the vibration testing equipment. To make sure that the observed third-order modes were accurate, ten accelerometers were spread out in the direction of the hit specimen's back (Figure 4). The impact's leading edge will be externally stimulated until the findings of the frequency measurements of the column become steady. It all started with the accelerometers taking readings of the pier's vibration properties during excitement; from there, the data was sent to the data logger; finally, the computer gathered the last time domain signal and converted it to frequency domain data using Fast Fourier Transform. The damaged column C1 gathered acceleration time-domain data, which are shown in Figure 4(c). The frequency of the damaged column's orders reduces, particularly at higher orders, as is easily seen. The optimal quantity of accelerometers to guarantee precise experiment results.

Table 1. Information of the components

Specimen	Longitudinal reinforcement ratio ρ_0 (%)	Hoop reinforcement ratio ρ_v (%)	Impact velocity at first-second-, third loading (V_1–V_2–V_3) (m/s)	Axial compression ratio ρ_a (%)
C1	10C20 (2.7)	8@50 (1.7)	4.5	30
C2			4.5–4.5–4.5	20
C3		8@100 (0.9)	4.5–4.5	20
C4		8@150 (0.5)	4.5	20

The axial compression ratio is calculated by $\rho_a = F_{axial}/(\pi r^2 f_c + A_s f_y)$.

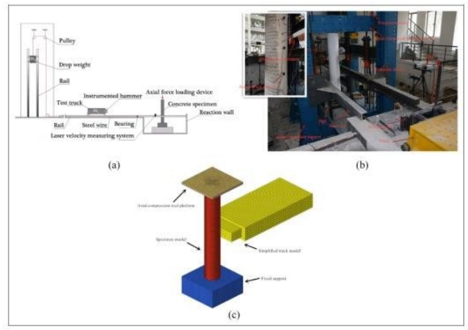

Figure 3. Impact testing system: (a) experimental test 2D view, (b) horizontal impact system, and (c) FE model of the RC column with the steel impactor.

Measurements of stiffness. This research will explain the stiffness variation using the total column stiffness as it is required to quantify the change in this parameter

$$0.5 \times (m_1 + m_2)v_0^2 + \mu m_1 g = m_2 g h \qquad (8)$$

but it is not possible to discriminate shear and bending stiffness throughout the experiment. The axial pressure was released after impact to guarantee

such that the top stiff plate separated from the column. At the very top of the column, the reaction wall delivered transverse forces of 100 kN, 200 kN, and 300 kN, in equal increments. As seen in Figure 5, where Dd stands for displacement differences, the force magnitude was measured by a dynamometer, and the displacement variations were documented by a displacement meter mounted on the column's top. Where E is the modulus of elasticity and I is the moment of inertia of the section, the calculation formula for the column stiffness was Equation (9).

ISSN2321-2152
www.ijmece .com
Vol 12, Issue 1, 2024

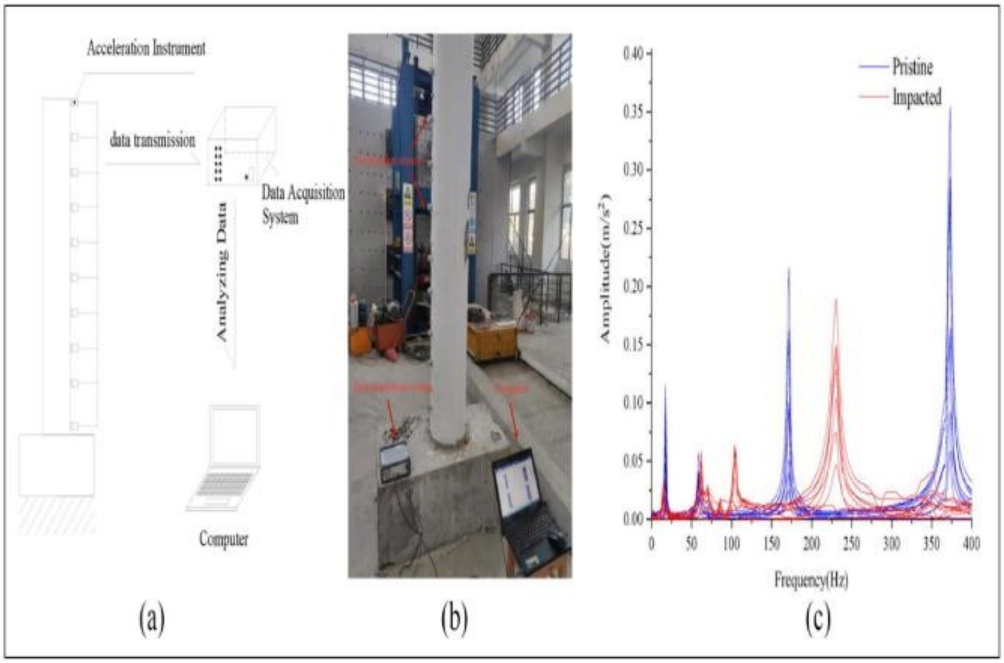

Figure 4. Modal testing system: (a) analytic flowcharts, (b) experimental facility, and (c) comparison of frequency response plots of post-impact and original RC piers.

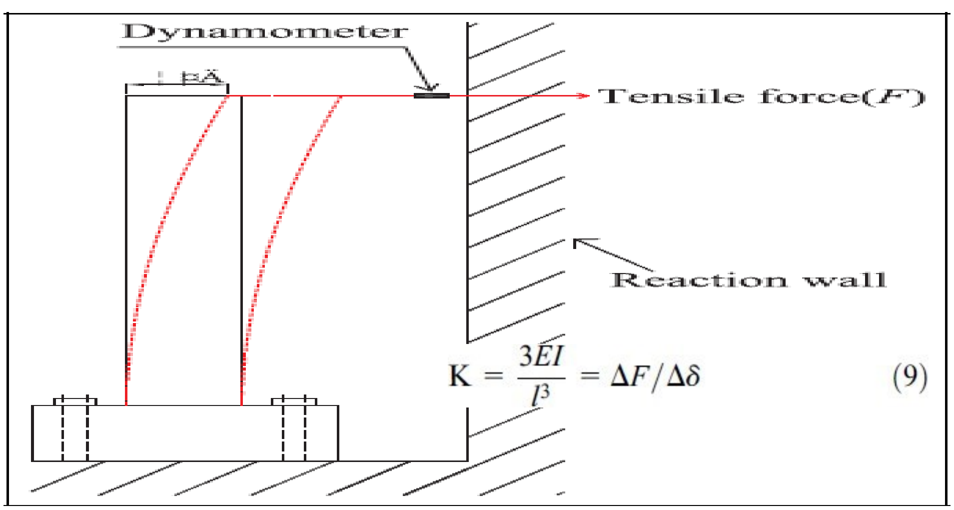

$$K = \frac{3EI}{l^3} = \Delta F/\Delta\delta \tag{9}$$

Figure 5. Stiffness measurement system.

5. Experimental results and analysis

Modal experiments. The findings of the experimental identifications of the natural frequencies are detailed in Figure 6 and Table 2 of this research. Sections where cracking occurred showed a reduction in stiffness due to the accumulated effects. The inherent frequencies were reduced in a non-monotonic manner when fractures formed.26 At low damage levels, the change in first-order frequency was insensitive, making it impossible to characterise the damage level. The results of the DCI calculations demonstrated that this index, taking into account multi-order modal frequencies, was very vulnerable to damage. The DCI will go up as damage becomes worse, which goes against the grain of how CoMAC has been evolving. utilising DCI as an assessment indicator is more logical than utilising merely the first-order modal frequency.

It was also impossible to disregard the shifts in the modal forms. Before and after the impact, Table 3 displays the findings of the modal shape measurement of Component C2. Variations in damage levels had little effect on the first-order mode form. It was possible to make an initial determination as to where the damage was located, however, by watching how the second-order and third-order mode forms changed. This spot had particularly many fissures, demonstrating how well the technique worked.

Impact experiments. Damage levels caused by component C2's three impact forces are correlated with changes in the temporal history, as shown in Figure 7. The column damage criticality index (DCI) rises and the peak impact force (PIF) falls as the damage severity grows. The peak impact force was found to be unaffected by the lower losses in the stiffness values. After two collisions, however, the pier's reactions were substantially weaker. The reactions were diminished due to the absence of column rigidity.

Stiffness verification. The changes in the values of the stiffness of the components before and after impact were obtained using the method described in Section ‘‘Stiffness measurement.’’Table 4 details the statistics of how quickly the stiffness values of each part are changing.

As a consequence of the impacts' effects on the overall structural stiffness, a number of natural frequencies shifted. This issue's emergence

Figure 6: Component modal frequencies:

first, the modal frequencies that are intact; second, the modal frequencies that are damaged.

Summary of modal tests (Table 2).

Specimens	Experimental			FEM			CoMAC	DCI
	Frequencies	DIFF (%)	Stiffness change (%)	FEM-PRED	Frequencies	DIFF (%)		
C1								
Undamaged			0	0		2.82	1	0
1st-order	19.53				18.98	10.29		
2nd-order	82.03				90.46	2.63		
3rd-order	210.99				205.44			
Impact-1			50.62	0.16		2.54	0.971	0.0001
1	17.57	−9.99			17.13	2.90		
2	75.70	−7.71			73.51	4.24		
3	188.95	−10.44			180.94			
C2								
Undamaged			0	0		2.82	1	0
1	19.53				18.98	12.74		
2	80.24				90.46	10.48		
3	229.49				205.44			
Impact-1			49.77	0.18		10.22	0.984	0.00255
1	19.08	−2.29			17.13	7.87		
2	79.79	−0.56			73.51	5.13		
3	190.73	−16.89			180.94			
Impact-2			68.29	0.23		2.68	0.966	0.01037
1	15.74	−19.36			15.32	2.80		
2	77.71	−3.15			75.53	6.66		
3	150.36	−34.48			140.35			
Impact-3			79.43	0.47		14.68	0.931	0.01858
1	15.74	−19.36			13.43	0.31		
2	50.78	−36.72			50.93	5.86		
3	99.60	−56.60			93.76			
C3								
Undamaged				0		1.21	1	0
1	19.21				18.98	2.80		
2	81.21				83.48	6.74		
3	208.73				194.67			
Impact-1			36.04	0.12		2.10	0.977	0.00005
1	17.58	−8.46			17.21	0.96		
2	74.30	−8.50			73.59	4.64		
3	186.31	−10.72			177.67			
Impact-2			46.92	0.33		3.80	0.963	0.00068
1	15.62	−18.67			15.03	2.25		
2	70.31	−13.42			71.89	2.61		
3	167.47	−19.76			171.85			

Table 2. (Continued)

Specimens	Experimental			FEM			CoMAC	DCI
	Frequencies	DIFF (%)	Stiffness change (%)	FEM-PRED	Frequencies	DIFF (%)		
C4								
Undamaged				0		2.29	1	0
1	17.57				17.98	30.51		
2	58.59				76.47	10.32		
3	169.99				187.53			
Impact-1			78.48	0.19		9.66	0.971	0.00094
1	15.48	− 11.91			13.98	14.73		
	53.54	−8.61			61.43	10.85		
3	138.67	− 18.42			153.71	2.82		

The DIFF: under the Experimental describes the initial frequency of the column and the frequency change after column damage; the DIFF: in the FEM describes the difference between the finite element calculation results and the experimental results.

Table 3. Comparison of the modal shapes of component C2.

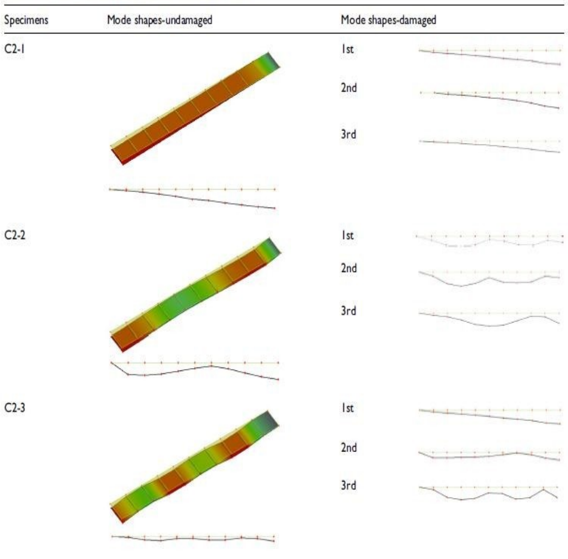

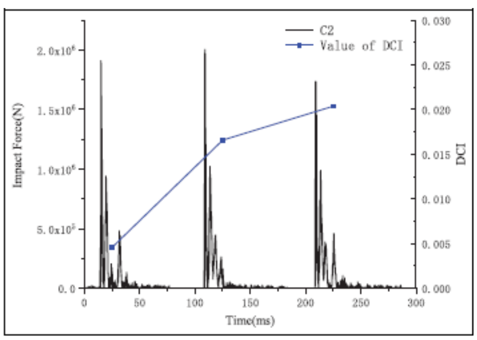

Figure 7. Comparison of the impact force time history and DCI changes of Component C2.

Table 4. Changes in the stiffness.

Specimen	Stiffness K (kn/m)	Change ratio (%)
C1		
Undamaged	8052.3	
C1-1	3976.4	50.62
C2		
Undamaged	7436.2	
C2-1	3734.8	49.77
C2-2	2357.7	68.29
C2-3	1529.6	79.43
C3		
Undamaged	6555.8	
C3-1	4192.8	36.04
C3-2	3479.6	46.92
C4		
Undamaged	6713.3	
C4-1	1444.6	78.48

first appeared in the system vibration equation as a characteristic value concern. Thus, the undamped mechanical system's motion equation (10) was used. The experimental model's initial third-order frequency approximation was resolved by means of the Rayleigh Method27, and the precision of the experimen- tal data was successfully verified. Therefore, in accor- dance with the principle of energy conservation, in which the strain energy at the maximum displacement time is equal to the initial kinetic energy, equation (11) was established.

$$\frac{\partial^2}{\partial x^2}\left[EI(x)\frac{\partial^2 v(x,t)}{\partial x^2}\right] + m(x)\frac{\partial^2 v(x,t)}{\partial t^2} = p(x,t) \quad (10)$$

$$U_{max} = W_{max} \quad (11)$$

The strain energy expression of a cantilever beam con- sidering only the displacement in one direction is as follows:

$$W_{max} = \frac{1}{2}\int_0^l EI\left(\frac{\partial^2 y}{\partial x^2}\right)^2 dx \quad (12)$$

The kinetic energy expression is as follows:

$$U_{max} = \frac{1}{2}\omega^2\int_0^l my^2(x)dx \quad (13)$$

Therefore, according to equations (10)–(13), the follow- ing was obtained:

$$\omega^2 = \frac{\int_0^l EI\left(\frac{\partial^2 y}{\partial x^2}\right)^2 dx}{\int_0^l my^2(x)dx} \quad (14)$$

In the current study, based on the above-mentioned method, the natural vibration frequencies of the cantile- ver components under the effects of gravity were solved and the first three order approximate solutions were determined as follows:

$$\omega_1 = \frac{3.5160}{l^2}\sqrt{\frac{EI}{m}}\omega_2 = \frac{22.0345}{l^2}\sqrt{\frac{EI}{m}}\omega_1 = \frac{61.6972}{l^2}\sqrt{\frac{EI}{m}} \quad (15)$$

The expressions of the structural stiffness were deter- mined (equation (16)), and the structural stiffness were C3 obtained using the calculations detailed in Table 4:

$$K = \frac{3EI}{l^3} \Rightarrow EI = \frac{Kl^3}{3} \quad (16)$$

In this study, we confirmed the reliability of the experiments by comparing them to the outcomes of the theoretical calculations. The results of the trials made it quite clear that the low-order frequencies were unaffected by the stiffness degradation phenomenon. Because of this, the actual numbers obtained did not match the answers that are roughly theoretical. To get better calculations, we need to apply elastic treatments to the borders as the experimental procedures used in this work couldn't guarantee stable fixed bounds. In spite of this, Figure 8 displays the experimentally shown acceptable relationships between DCI and stiffness changes. Hence, it was thought that in engineering, the degree of stiffness loss could be correctly predicted from the recorded changes in component frequencies.

Table 5. Comparison of the theoretical calculations and the experimental data.

Specimens	Frequencies (HZ)								
	1st			2rd			3nd		
	Theo	Exp	Error (%)	Theo	Exp	Error (%)	Theo	Exp	Error (%)
C1	13.30	19.531	31.903	83.38	82.031	−1.645	233.46	210.993	−10.648
C1-1	9.35	17.578	46.809	58.59	75.703	22.605	164.06	188.953	13.174
C2	12.79	19.531	34.514	80.12	80.242	0.152	224.35	229.492	2.241
C2-1	9.06	19.083	52.523	56.78	79.791	28.839	159.00	190.736	16.639
C2-2	7.20	15.749	54.283	45.12	77.717	41.943	126.33	150.365	15.984
C2-3	5.80	15.749	63.172	36.34	50.781	28.438	101.75	99.609	−2.149
C3	12.00	19.213	37.542	75.23	81.212	7.366	210.65	208.73	−0.920
C3-1	9.60	17.588	45.417	60.16	74.304	19.035	168.47	186.314	9.577
C3-2	8.75	15.625	44.000	54.81	70.313	22.049	153.47	167.476	8.363
C4	12.15	17.578	30.880	76.13	58.594	−29.928	213.17	169.992	−25.400
C4-1	5.64	15.484	63.575	35.32	53.547	34.039	98.89	138.672	28.688

In the table, C2-1 represents the experimental data of the C2 member following the first impact; Test represents the experimental result.

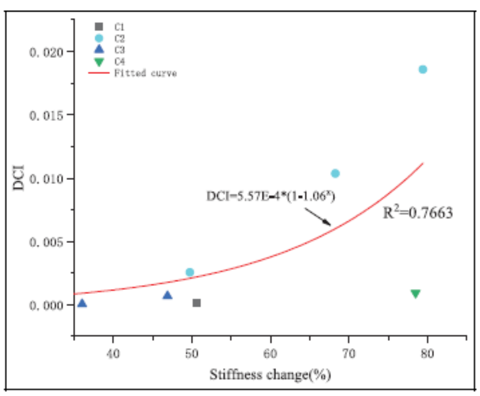

Figure 8. Correlations between the DCI and stiffness losses.

Numerical simulation and discussion

Using the commercial program LS-DYNA, a finite element model was created that matched the experiments. Modal analysis follows collision analysis via implicit analysis. In this part, the solution to the algorithm conversion problem is detailed, and the finite element model is calibrated.

Finite element (FE) model

Figure 3(c) displays the 3D nonlinear finite element analysis model that was used, which was based on the experimental model. The impacting vehicles made of steel and concrete used hexahedral elements with one integral point, while the reinforcements were 2 3 2 Gauss integral elements from Hughes-Liu sectional beams. A piecewise nonlinear model was also a reasonable way to characterise the longitudinal reinforcements and the stirrups, which were considered elastic-plastic materials. To account for the impacts of strain rate, this research made use of the dynamic intensification factor (DIF) relationships given by Li and Hao28. Using equation (17), we were able to determine the correlations between strain rates and DIF. A multi-stage elastic-plastic curve was used to characterise the model. Under quasi-static circumstances, the material state description was denoted by DIF = 1 in the present research. When the stress level reaches 350 MP and the strain reaches 0.2%, the material shifts from an elastic to a plastic condition, which corresponds to the yield point. Figure 3(b) shows that the experimental superstructure was an axial hydraulic loading platform. To apply the gravity load to the entire model, the numerical model used the keyword *LOAD BODY Z. At the same time, an elastic material of appropriate mass was used to simplify the model. One way to modify the elastic material's mass is to alter its thickness. Similarly, the steel trolley was treated as an elastic material for the sake of calculations as its rigidity was much lower than that of the RCC structure. The material specifications are detailed in Table 6:

$$\mathrm{DIF_s} = \left(\frac{\dot{\varepsilon}}{10^{-4}}\right)^{0.074-0.040\frac{f_y}{414}} \qquad (17)$$

In the current study, LS-DYNA contact keyword *CONTACT_SURFACE TO SURFACE contact algo- rithm was used between the mass object and column, and the keyword named *CONTROL_DYNAMIC_ RELAXATION was used for the dynamic relaxation analysis of the structure 0.1 s prior to the calculation in

Table 6. Model material parameters.

Type	Material modal	Parameter	Magnitude
Longitudinal rebar	PIECEWISE_LINEAR_PLASTICITY (*MAT_024)	Mass density	7850 kg/m^3
		Modulus of elasticity	205,000 Mpa
		Poisson's ratio	0.3
		Yield stress	400 MPa
		Failure strain	0.4
Stirrup	PIECEWISE_LINEAR_PLASTICITY (*MAT_024)	Density	7850 kg/m^3
		Modulus of elasticity	205,000 Mpa
		Poisson's ratio	0.3
		Yield stress	335 MPa
		Failure strain	0.4
Steel plates, Steel impactor	ELASTIC (*MAT_03)	Mass density	7850 kg/m^3
		Modulus of elasticity	205,000 Mpa
		Poisson's ratio	0.3
Concrete	CSC Modal (*MAT_159)[22]	Mass density	2490 kg/m^3
		Compressive strength	42 MPa
		Maximum aggregate size	15 mm
		EROD	1.1
		RECOV	10.4

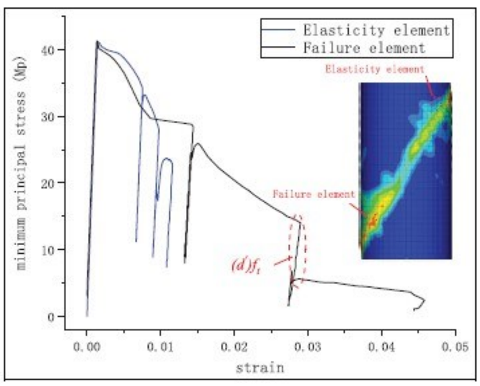

Figure 9. Cylinder model and result diagram.

in order to make sure the axial force application is stable. Next, the concrete grid size was kept at 10 mm according to the findings of Yuan et al.29, who studied the effect of grid size sensitivity. Not only that, but the steel impact trolley might be considered a rigid body due to the little deformations it acquired during contact procedures. For that reason, 50 mm squares were used to partition it. In order to account for the slip effects between the reinforced concrete, the contact setting between the reinforcement and the concrete was set to CONSTRAIN_BEAM IN SOLID.

Concrete material model validation

The fact that the plastic deformation may be properly assessed and that unloading stress can occur reasonably is the key to proving that CSC is modal. As seen in Figure 9, this section pertains to the simple finite element model of the F150*300 mm cylinder that was suggested by Malvar,30. Research using axial compression on the

the displacement technique was used to model cylinders and perform cyclic loading. Earlier, we covered the material parameter settings. In Figure 9, we can observe the stress-strain development process of the elastic element and the failure element during loading. By comparing these data with experimental and finite element model results from literature, we can see that the model successfully captures the effects of stiffness degradation during damage accumulation processes. In a similar vein, the concrete constitutive model underwent trial calculations using the previously created experimental model. The experimental findings were compared with the numerical calculation results, and Figure 10 depicts the time history of the impact force and fracture formation of Component C4. In low-velocity impact scenarios, the findings demonstrated that the constitutive model could accurately forecast both the peak impact force and its evolution. Results from both the calculations and the experiments were found to be within a 10% margin of error.

Modal analysis of damaged model

Due to the oblique punching cracks (Figure 10) which occurred after impact, pre-existing damages were required in the numerical calculations. The pre-existing damage (PRED) parameters provided by the CSC model reasonably solved this issue. Modal analysis was

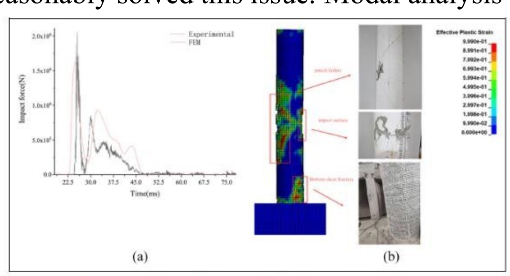

Figure 10. Experimental results of Component C4 and comparison of the value calculation results: (a) dynamic responses of specimens C4 and (b) impact damage of specimens C4.

Table 7. Comparison of the modal frequencies under different damage degrees.

Model frequencies/ PRED	0	0.1	0.3	0.5	0.7
1st	22.3851	21.57	19.67	17.50	15.57
2nd	98.4437	94.48	85.58	75.70	63.98
3nd	230.4552	217.99	192.20	162.93	126.98

ISSN2321-2152
www.ijmece .com
Vol 12, Issue 1, 2024

Table 7 displays the outcomes of the same computation model run with varying PRED values. The results showed that the modal frequencies decreased nonlinearly as the PRED values increased.
Research on RC piers' cumulative damage issues and modal analysis is now within reach, thanks to restart technology. These issues were investigated experimentally and numerically by Kishi et al.33. Nevertheless, KISHI's approach was limited to collisions involving simple rigid bodies and could not address the challenges posed by nonlinear big deformation impacts involving complicated structures and several failure variables. Hence, the following is a novel restart approach that was provided by this study:
1. One thing that was done after the first calculation was to compare the experimental data with the results of the calculations that had been run via the post-processing program Ls-Prepost. Upon verification of accurate calculation results, the OUTPUT option in Ls-Prepost was used to generate data such as the element and nodes. This data may then be utilised in a geometric model for further calculations.

2. Simultaneously, the stress and plastic strain of each element were output using the DYNAIN option in Ls-Prepost after the first calculation was finished. The material was initially damaged in order to create a stress-strain initialisation file at the start of the second calculation.

3. The second impact file was obtained by resetting the solution settings, assembla-geometry file, and stress initialisation file. During the construction of the modal analysis files, it was possible to appropriately simplify the model by deleting the top steel plate and steel trolley and by setting the solver to implicit analysis, among other things.

In this study, we tweaked the PRED parameters to make sure the MAC values were accurate so that the modal calculations would be reliable.

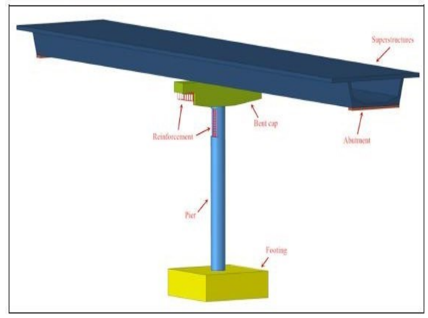

Figure 11. Specific sizes of the pier models.

were within a reasonable range. Then, the range was divided in order to facilitate the calculation process. Table 7 shows the numerical calculated modal frequency values. The results show that the calculation method is suitable for the present study.

Vehicle-bridge impact model

In addition, the DCI may provide engineering designs with references. Columns with varying section sizes, impact velocities, and vehicle masses were used in a large number of numerical simulation calculations to study the relationships between dynamic responses and modal frequencies of bridge piers under the effects of cumulative impacts of vehicles. At the moment of collision, the findings revealed two kinds of forces that could be controlled by the values of cargo mass and velocity. The results of the experiments allowed for the determination of the correct parameters for the finite element analysis. Next, the DCI damage indicators used in this research will be cross-referenced with a full-scale model of the pier and the Ford F800 medium truck model created by the National Crash Analysis Centre (NACA). Researchers looked at the correlation between damage severity and dynamic response using regression analysis.
Details on the watercraft and docks Using the identical material model, contact mode, and strain rate effect parameters as specified in Section "Concrete Material Model Validation," this analysis confirmed the finite element model's validity. In their proposal, Consolazio et al. suggested a bridge model that includes a

By simplification of the prototype issue to include a single column, a superstructure, and two supports, the dynamic response of a multi-span bridge may be efficiently predicted using bridge columns and two spans. Figure 11 shows the dimensions of the concrete foundation, which were 5000 mm x 5000 mm x 1200 mm. A trapezoidal solid beam was placed on top of the column to transfer the weight of the 30-meter-long superstructure to the pier column. To keep the axial compression ratio constant in all collision situations, its weight was adjusted according to the column section size. Table 8 displays all instances of collisions. The column was fastened to the bridge pier superstructure using rubber bearings. Previous studies conducted by EI-TAWIL et al. shown that the total dynamic response of the pier is unaffected by the stiffness of the support. In this case, we'll use the LS-DYNA keyword "CONTACT AUTOMATIC SURFACE TO SURFACE" to presume that the pier's vertical section will touch the concrete surface.

The Ford vehicle model was used to depict the collision with the bridge pier, as seen in Figure 12. The model was shared and tested for correctness by Abdelkarim et al.11 and Sharma et al.21. With an engine mass of 0.24 t and a payload mass of 2.8 t, the Ford truck had a total mass of 8 t in the model used in this investigation. We used elastic materials with moduli strengths of 11,000 and 2000 for the engine and cargo simulations, respectively. Altering the product quality allowed us to regulate the vehicle model's weight.

Vehicle impact responses

Peak impact force (PIF). The change of damage degree is reflected by cumulative impact.. The typical time

Table 8. Numerical simulations of the component information.

scenarios	Column size (mm)	Longitudinal reinforcement ratio ρ_0 (%)	Hoop reinforcement ratio ρ_v (%)	Axial compression ratio ρ_a (%)
C800-V60-W8	800	10C22 (0.756)	25@150 mm (1.31)	388 *t* (40.5)
C800-V90-W8				
C800-V110-W8				
C1000-V60-W8	1000	10C28 (0.784)	25@150 mm (1.08)	612.95 *t* (40.5)
C1000-V90-W8				
C1000-V110-W8				
C1200-V60-W8	1200	10C32 (0.711)	25@150 mm (0.95)	859.6 *t* (40.5)
C1200-V90-W8				
C1200-V110-W8				
C1200-V60-W10				
C1200-V90-W10				
C1200-V110-W10				
C1200-V60-W12				
C1200-V90-W12				
C1200-V110-W12				

In the table, C800-V60-W8-1 indicates that the 800 mm diameter column is the first to be impacted by the vehicles with a total weight of 8 *t* and a speed of 60 km/h; 10C22 means 10 steel bars with a diameter of 22 mm; 25@150 means that the stirrup spacing is 150 mm and the diameter is 25 mm.

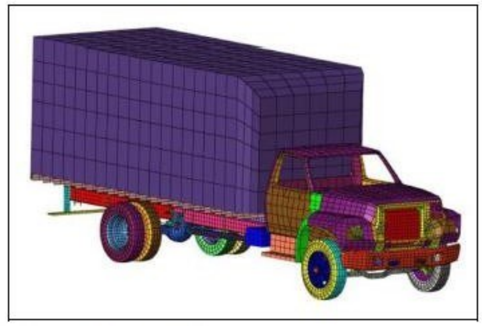

Figure 12. Truck model.

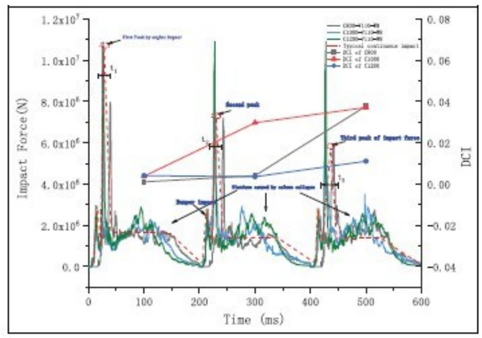

Figure 13. Time history diagram of the typical continuous impact force and damage degrees of the bridge piers.

The DCI values and impact histories of the three sequential events are shown in Figure 13. Figure 8 shows a temporal analysis of the V110-W8 component's three impact forces (C800, 1000, and 1200). With a 200 ms computation time for each hit, the second impact ended at 400 ms and the third impact began at 200 ms, respectively. The engine's collision with the bridge pier was the common cause of the three impact forces' maximum values. Hence, the results of the comparison showed that the first typical impact force's time history diagram was in agreement with the shape of the impact force's time history diagram created by Cao et al.35 and Chen et al. 34. Using the effective plastic strain after impact, Figure 14 explains the degree of component damage. As the impact periods added up, the component modal parameters deviated from their starting states, and as stiffness values decreased, PIF values decreased as well. Researchers determined that this occurrence was typical of damaged piers. It should be mentioned that this

ISSN2321-2152
www.ijmece .com
Vol 12, Issue 1, 2024

C1200-V110- W8 did not exhibit this behaviour. The reason for this was that the stiffness values of the medium-sized pier were not significantly affected by the impacting impacts of the vehicle travelling at such speed. The findings demonstrate that DCI values, as seen in Figures 13 and 14, rise with increasing degree of damage. Exhibit the efficacy of DCI pier damage detection for a more robust resistance to piers, whose value increases at a slower pace.

Results from numerical simulations of columns of varying sizes are detailed statistically in Table 9, which also includes peak values, duration Tn, and 25 ms.

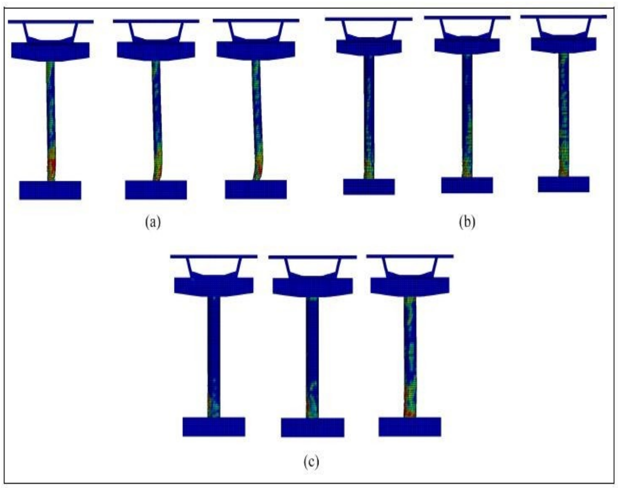

Figure 14. Comparison of the impact damage degrees: (a) C800-V110-W8, (b) C1000-V110-W8, and (c) C1200-V110-W8.

Table 9. Numerical simulation results.

Scenarios	First impact			Second impact			Third impact		
	PIF (MN)	ESF (MN)	DCI	PIF	ESF	DCI	PIF	ESF	DCI
C800-V60-W8	2.27	1.510	0.00033	2.52	1.546	0.00546	2.4	1.537	0.00736
C800-V90-W8	7.08	2.069	0.00060	6.35	2.131	0.01363	7.16	2.092	0.02769
C800-V110-W8	9.88	2.175	0.00105	7.86	2.526	0.01641	5.85	2.752	0.03779
C1000-V60-W8	2.12	1.450	0.00028	2.22	1.494	0.00058	2.13	1.530	0.00104
C1000-V90-W8	8.2	2.314	0.00069	6.73	2.337	0.00186	7.06	2.225	0.01035
C1000-V110-W8	10.9	2.423	0.00379	7.85	2.852	0.02971	6.38	2.714	0.03709
C1200-V60-W8	3.01	1.621	0.00019	3.23	1.634	0.01150	2.75	1.507	0.02445
C1200-V90-W8	8.89	2.224	0.00054	8.16	2.106	0.00103	6.4	2.178	0.00901
C1200-V110-W8	10.7	2.549	0.00411	10.7	2.532	0.00355	7.93	2.533	0.01107
C1200-V60-W10	3.07	1.601	0.00004	2.62	1.537	0.00121	2.70	1.554	0.00335
C1200-V90-W10	8.01	2.374	0.00025	6.08	2.350	0.00177	7.85	2.428	0.01308
C1200-V110-W10	11.9	2.523	0.00749	8.89	2.687	0.014437	8.39	2.428	0.02547
C1200-V60-W12	3.14	1.595	0.00029	2.57	1.549	0.002741	2.95	1.563	0.01451
C1200-V90-W12	8.14	2.253	0.00643	7.34	2.297	0.017594	4.37	2.181	0.02314
C1200-V110-W12	12.20	2.553	0.00314	6.39	2.731	0.019881	6.32	2.662	0.02495

equivalent static calculation results of each impact force. All of the components in the table were impacted by a medium-sized vehicle of 8 t, which represented a typical type of engine impact scenario.
The studies conducted by EI-TAWIL [40] showed that the peak force formula (equation (18)) of ship- bridge impacts provided by American Association of State Highway and Transportation Officials (AASHTO) was also applicable to vehicle impacts. The impact velocity V (m/s) and the mass W (kg) of the impacting bodies were considered in the formula. In this study, a new expression equation (20) was pro- posed for the pre-damaged impact problem, and two dimensionless parameters, damage factor DCI, and the

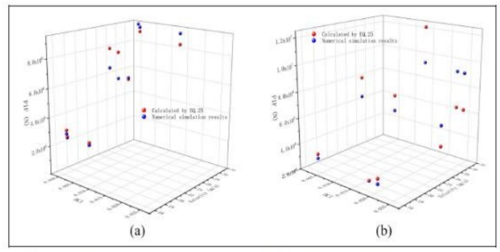

Figure 15. Comparison between simulation results and equation (20): (a) C1200-W10 and (b) C1200-W12.

equivalent stiffness (b/800) were introduced. Therefore, the formula was able to achieve a more comprehensive description of each parameter. Five regression coeffi- cients (referred to as a, b, c, d, and e) were determined using a nonlinear regression analysis method. It was found that when subjected to continuous impacts, the PIF engine could be estimated using equation (20). Figure 15 details this study's comparison of the fitting results and the numerical simulation results

$$F_i = f\{\alpha(V)^{\beta}(W)^{\gamma}\} \quad (18)$$

$$PIF = f\left\{a(DCI)^{b}(V)^{c}(W)^{d}\left(\frac{b}{800}\right)^{e}\right\} \quad (19)$$

$$PIF_{engine} = 10027.08(DCI)^{-0.044}(V)^{2.13}(W)^{-0.085}\left(\frac{b}{800}\right)^{0.364} \quad (20)$$

6. Conclusion

7. The damage and structural safety of the bridge piers impacted by low-speed vehicles were assessed using the frequency domain-based correlation approach (DCI), which was developed in this study. We confirmed its usefulness and feasibility. Based on the results, the researchers came to these conclusions: 1. The modal frequency parameters of the structures were obtained by fast Fourier transform (FRFs) processing. The major approaches in the suggested strategy were the measurements of the frequency response functions of the structures with impact damages. The discovery of cracking

columns' intrinsic frequencies were significantly impacted by procedures. The impacts also reduced the columns' stiffness values at the fracture sections and caused nonmonotonic decreases in the modal frequencies. This means that structural damage correlation indexes (DCIs) may be calculated and compared using the collected data. The results proved that the DCI was capable of accurately predicting both the residual stiffness values and the extent of structural damage.

2. The credibility of the reference experimental model is confirmed, and methods for calculating modal identification after structural damage and impact on reinforced concrete columns based on the finite element approach are presented.

3. The predamaged vehicle-pier impact events were computed using a finite element approach in the present research inquiry. To determine the maximum impact force, the DCI was used in conjunction with equation (20). The suggested formula outperformed the results of comparable studies because it accounted for the decreases in impact force and the loss of stiffness due to structural flaws. This meant that subsequent stages of structural design may benefit from the suggested approach.

References

1. Cook W, Barr PJ and Halling MW. Bridge failure rate. J Perform Constr Facil 2015; 29: 04014080.

2. Gomes GF, Mende´z YAD, Alexandrino PSL, et al. The use of intelligent computational tools for damage detec- tion and identification with an emphasis on composites: a review. Compos Struct 2018; 196: 44–54.

3. Perez MA, Gil L and Oller S. Impact damage identifica- tion in composite laminates using vibration testing. Com- pos Struct 2014; 108: 267-276.

4. Zenzen R, Belaidi I, Khatir S, et al. A damage identifica- tion technique for beam-like and truss structures based on FRF and Bat algorithm. CR Me´canique 2018; 346: 1253–1266.

5. Liu S, Zhang L, Chen Z, et al. Mode-specific damage identification method for reinforced concrete beams: con- cept, theory and experiments. Constr Build Mater 2016; 124: 1090–1099.

6. Sha G, Cao M, Radzien´ski M, et al. Delamination- induced relative natural frequency change curve and its use for delamination localization in laminated composite beams. Compos Struct 2019; 230: 111501.

7. Sampaio RPC, Silva TAN, Maia NMM, et al. Damage identification based on response functions in time and frequency domains. In: Nobari AS and Ferri Aliabadi MH (eds) Vibration-based techniques for damage detection and localization in engineering structures. China: World Scientific Publishing Co Pte Ltd, 2018, pp. 197–236.

8. Pe´rez MA, Pernas-Sa´nchez J, Artero-Guerrero JA, et al. High-velocity ice impact damage quantification in com- posite laminates using a frequency domain-based correla- tion approach. Mech Syst Signal Process 2021; 147: 107124.

9. Officials AAoSHaT. AASHTO-LRFD. Bridge design specifications – customary US Units. 5th ed. Washington, DC: Officials AaoSHaT, 2010.

10. Chen L, El-Tawil S and Xiao Y. Reduced models for simulating collisions between trucks and bridge piers. J Bridge Eng 2016; 21: 04016020.

11. Abdelkarim OI and ElGawady MA. Performance of bridge piers under vehicle collision. Eng Struct 2017; 140:337–352.
12. Al-Thairy H and Wang YC. An assessment of the current Eurocode 1 design methods for building structure steel columns under vehicle impact. J Constr Steel Res 2013; 88: 164–171.
13. Buth CE, Brackin MS, Williams WF, et al. Collision loads on bridge piers: phase 2, report of guidelines for designing bridge piers and abutments for vehicle collisions. Bryan, TX: Texas Transportation Institute, 2011.
14. Buth CE, Williams WF, Brackin MS, et al. Analysis of large truck collisions with bridge piers: phase 1, report of guidelines for designing bridge piers and abutments for vehicle collisions. Bryan, TX: Texas Transportation Insti- tute, 2010.
15. Chen L, Xiao Y, Xiao G, et al. Test and numerical simu- lation of truck collision with anti-ram bollards. Int J Impact Eng 2015; 75: 30–39.
16. Cai J, Ye JB, Chen QJ, et al. Dynamic behaviour of axially-loaded RC columns under horizontal impact loading. Eng Struct 2018; 168: 684–697.
17. Zhou XW, Zhou M, Gao YS, et al. An evaluation study on the cumulative impact damages of reinforced concrete piers based on modal frequencies. Eng Fail Anal 2021; 119: 104983.
18. Adhikary SD, Li B and Fujikake K. Dynamic behavior of reinforced concrete beams under varying rates of con- centrated loading. Int J Impact Eng 2012; 47: 24–38.
19. Pham TM and Hao H. Influence of global stiffness and equivalent model on prediction of impact response of RC beams. Int J Impact Eng 2018; 113: 88–97.
20. Chen L, Wu H and Liu T. Shear performance evaluation of reinforced concrete piers subjected to vehicle collision. J Struct Eng 2020; 146: 04020026.
21. Sharma H, Hurlebaus S and Gardoni P. Performance- based response evaluation of reinforced concrete columns subject to vehicle impact. Int J Impact Eng. 2012; 43: 52–62.
22. Murray YD. Users manual for LS-DYNA concrete material model 159. No. FHWA-HRT-05-062. Washing- ton, DC: United States Federal Highway Administration Office of Research, Development, and Technology, 2007.
23. Pastor M, Binda M and Harcˇarik T. Modal assurance cri- terion. Procedia Eng 2012; 48: 543–548.
24. Allemang RJ. The modal assurance criterion – twenty years of use and abuse. Sound Vib 2003; 37: 14–23.
25. Ahlgren P, Jarneving B and Rousseau R. Requirements for a cocitation similarity measure, with special reference to Pearson's correlation coefficient. J Am Soc Inform Sci Technol 2003; 54: 550–560.